

# Coulomb crystals in the magnetic field

D. A. Baiko

*A.F. Ioffe Physical-Technical Institute, Politekhnikeskaya 26,*

*194021 St.-Petersburg, Russian Federation*

(Dated: October 1, 2009)

The body-centered cubic Coulomb crystal of ions in the presence of a uniform magnetic field is studied using the rigid electron background approximation. The phonon mode spectra are calculated for a wide range of magnetic field strengths and for several orientations of the field in the crystal. The phonon spectra are used to calculate the phonon contribution to the crystal energy, entropy, specific heat, Debye-Waller factor of ions, and the rms ion displacements from the lattice nodes for a broad range of densities, temperatures, chemical compositions, and magnetic fields. Strong magnetic field dramatically alters the properties of quantum crystals. The phonon specific heat increases by many orders of magnitude. The ion displacements from their equilibrium positions become strongly anisotropic. The results can be relevant for dusty plasmas, ion plasmas in Penning traps, and especially for the crust of magnetars (neutron stars with superstrong magnetic fields  $B \gtrsim 10^{14}$  G). The effect of the magnetic field on ion displacements in a strongly magnetized neutron star crust can suppress the nuclear reaction rates and make them extremely sensitive to the magnetic field direction.

PACS numbers: 26.60.Gj, 67.80.-s, 52.27.Aj, 52.27.Lw, 52.25.Xz

## I. INTRODUCTION

The model of a crystal of point-like charges immersed in a uniform neutralizing background of opposite charge was conceived by Wigner [1] to describe a possible crystallization of electrons. These Wigner crystals of electrons have much in common with Coulomb crystals of ions with the uniform electron background. The model of the Coulomb crystal is widely used in different branches of physics, including theory of plasma oscillations (e.g., [2]), solid state physics, and works on dusty plasmas and ion plasmas in Penning traps (e.g.,

[3]).

Moreover, Coulomb crystals of ions, immersed in an almost uniform electron background, are formed in the cores of white dwarfs and envelopes of neutron stars. The properties of such crystals are important for the structure and evolution of these astrophysical objects (e.g., [4, 5]). In particular, the Coulomb crystal heat capacity [6] controls cooling of old white dwarfs and is used to determine their ages (e.g., [7]). Crystallization of white dwarfs can influence their pulsation frequencies. It can thus be studied by powerful methods of asteroseismology [8]. Microscopic properties of Coulomb crystals determine the efficiency of electron-phonon scattering in white dwarfs and neutron stars, and, hence, transport properties of their matter (such as electron thermal and electric conductivities, and shear viscosity, e.g., [9, 10]) as well as the neutrino emission in the electron-ion bremsstrahlung process [11]. Many-body ion correlations in dense matter produce screening of ion-ion (nucleus-nucleus) Coulomb interaction and affect nuclear reaction rates in the thermonuclear burning regime with strong plasma screening and in the pycnonuclear burning regime (when the reacting nuclei penetrate through the Coulomb barrier owing to zero-point vibrations in crystalline lattice). The description of various nuclear burning regimes and observational manifestations of burning in white dwarfs and neutron stars are discussed in Refs. [12, 13, 14] and references therein. The manifestations include type Ia supernova explosions of massive accreting white dwarfs, bursts and superbursts, deep crustal heating of accreted matter in neutron stars.

Since the late 1990s certain astrophysical applications have been requiring a comprehensive study of Coulomb crystals in strong magnetic fields. The topic has become important due to the growing observational evidence that some very intriguing astrophysical objects, soft-gamma repeaters (SGRs) and anomalous X-ray pulsars, belong to the same class of sources called magnetars (see, e.g., [15, 16, 17] and reference therein). These are thought to be isolated, sufficiently warm neutron stars with extremely strong magnetic fields  $B \gtrsim 10^{14}$  G. For instance, the magnetic field of SGR 1806–20, inferred from measurements of its spin-down rate, is  $B \sim 2 \times 10^{15}$  G [18]. Magnetars are observed in all ranges of the electromagnetic spectrum. They show powerful quasipersistent X-ray emission, bursts and giant bursts with enormous energy release. During giant bursts, one often observes quasi-periodic X-ray oscillations which are interpreted (e.g., [19]) as vibrations of neutron stars (involving torsion vibrations of crystalline neutron star crust). It is likely that the activity of magnetars is powered by their superstrong magnetic fields. Thus the magnetars can be

viewed as natural laboratories of dense matter in magnetic fields. In order to build adequate models of magnetar envelopes and interpret numerous observations, it is crucial to know the properties of magnetized Coulomb crystals. The main goal of this paper is to study in detail Coulomb crystals in an external uniform magnetic field. (The results reported here were partially presented in [20].)

The Coulomb crystals in question consist of fully ionized ions with charge  $Ze$  and mass  $M$  arranged in a crystal lattice and immersed into the rigid electron background (in this case, rigid means unpolarizable or incompressible, i.e. constant and uniform). The effect of the magnetic field  $B$  on the ion motion can be characterized by the ratio

$$b = \omega_B / \omega_p, \quad (1)$$

where

$$\omega_B = \frac{ZeB}{Mc}, \quad \omega_p = \sqrt{\frac{4\pi Z^2 e^2 n}{M}} \quad (2)$$

are the ion cyclotron frequency and the ion plasma frequency, respectively;  $n$  is the ion number density, while  $c$  is the speed of light. It is expected that the magnetic field modifies the properties of the ion crystal at  $b \gtrsim 1$  (see, however, Figs. 2 and 8 below). In a strong magnetic field the approximation of rigid electron background is a bigger idealization of the real situation in neutron star crust matter, since higher densities are required to achieve full ionization and suppress the polarizability of the electron background. The higher densities (and  $\omega_p$ ) imply smaller  $b$ . However, the effective ion charge approximation turns out to be successful for analyzing partially ionized systems (e.g., [21]). The quantity  $b$  (also equal to  $v_A/c$ , where  $v_A = B/\sqrt{4\pi\rho}$  is the Alfvén velocity,  $\rho$  being the mass density) is, actually, independent of the ion charge. Hence, one can consider large  $b$  in Coulomb crystals at not too high densities having in mind the effective ion charge approximation. Despite that, the effect of the polarizability of the compensating electron background has to be studied separately.

The closely related problem of magnetized Wigner crystals of electrons was studied in the early 1980s by Usov, Grebenshikov and Ulinich [22] and by Nagai and Fukuyama [23, 24]. Usov et al. [22] obtained the equations for crystal oscillation modes, studied qualitatively the oscillation spectrum, and diagonalized the Hamiltonian of the crystal for a proper quantum description of the oscillations in terms of phonons. In addition, the authors investigated asymptotic temperature and magnetic field dependences of the specific heat, rms electron

displacement from the respective lattice site, and magnetic moment of the crystal. They obtained a soft phonon mode with the frequency  $\Omega \propto k^2$  near the center of the Brillouin zone. It resulted in a rather unusual low-temperature specific heat behavior ( $T^{3/2}$ ) instead of the standard Debye law ( $T^3$ ). Also, the authors mentioned the dependence of the crystal energy on the magnetic field direction as well as the increased stability of the crystal due to a suppression of electron vibration amplitudes. In addition, Usov et al. [22] considered the dielectric function of the crystal and studied the effect of the electromagnetic field induced by the electron motion. Their main results were, however, of semi-qualitative nature, limited to various extreme cases, whereas the present paper focuses mostly on quantitative results, pertaining to Coulomb crystals of ions, with an eye to astrophysical implications.

Nagai and Fukuyama [23] calculated phonon spectra of magnetized body-centered cubic and face-centered cubic (bcc and fcc) Wigner crystals and compared the energies of these crystals at zero temperature as a function of the magnetic field. The crystal energy was calculated as a sum of the electrostatic (Madelung) energy, and the zero-point energy of crystal vibrations. The effect of the anharmonic and exchange terms was neglected. The electrostatic energy is independent of the magnetic field (as long as the field does not alter the lattice structure). The vibration energy does depend on the field because the field modifies phonon modes. At zero field the energy minimum is realized by the bcc structure, both with and without zero-point vibrations (in general, it is not true for polarizable background, e.g., [25]). The authors showed that for a sufficiently strong magnetic field and at relatively high densities [ $r_s < 275$ , where  $r_s = a_e/a_0$  is the standard density parameter,  $a_e = (3/4\pi n_e)^{1/3}$ , and  $a_0$  is the Bohr radius,  $n_e$  being the electron number density] the full energy is minimized by the fcc structure. It is worth mentioning that the authors did not consider the dependence of the zero-point energy on the magnetic field direction and performed all calculations for a fixed direction (along one of the high symmetry axes of the crystals). However, this choice of the field direction for the bcc lattice was not optimum, as far as the lattice energy was concerned. Moreover, the energy gain obtained by choosing the optimum direction is of the same order of magnitude as the difference between the zero-point energies of bcc and fcc lattices.

Nagai and Fukuyama [24] investigated an analogous structural transition between bcc and hexagonal close-packed (hcp) electron Wigner lattices. The hcp lattice was found energetically favorable for a sufficiently strong magnetic field at  $r_s < 10700$ . This result seems

more robust since the energy difference between bcc and hcp lattices is several times larger than the energy gain obtained by choosing the optimum direction of the magnetic field in the bcc lattice (the field direction adopted in [24] was the same as in [23]).

In addition, Nagai and Fukuyama [24] described the behavior of all 6 phonon modes of the hcp lattice in the magnetic field. Also, they analyzed quantitatively the behavior of transverse and longitudinal electron displacements from the equilibrium positions for bcc and hcp lattices (at zero temperature) and concluded (qualitatively) that in strong magnetic fields the crystals became significantly more stable in the transverse direction and somewhat more stable in the longitudinal direction.

The present paper is organized as follows. Section II discusses equations for Coulomb crystal oscillations in the magnetic field. Section III focuses on the phonon spectrum of such a crystal with a simple lattice (i.e., one ion in the primitive cell). The Hamiltonian of the system is diagonalized in Sec. IV, which allows one to express the ion displacement operator via phonon creation and annihilation operators. Section V presents numerical calculations of thermodynamic functions of the Coulomb bcc crystal for a wide range of densities, temperatures and magnetic fields. In Sec. VI these results are applied to the real physical system found in magnetar crust. Section VII is devoted to an analysis of the rms amplitudes of ion vibrations and to the Debye-Waller factor of the magnetized Coulomb crystal. Finally, Sec. VIII considers the dependence of phonon spectrum moments on the magnitude and direction of the magnetic field.

The results will be parameterized by the quantum parameter  $\theta = \hbar\omega_p/T \equiv T_p/T$  (where  $T$  and  $T_p$  are temperature and ion plasma temperature, respectively), and by the Coulomb coupling parameter  $\Gamma = Z^2e^2/(aT)$ . In this case,  $a = (3/4\pi n)^{1/3}$  is the ion sphere radius. The Boltzmann constant is set equal to  $k_B = 1$ .

## II. DISPERSION EQUATION IN THE MAGNETIC FIELD

Let us consider a Coulomb crystal of ions in a uniform magnetic field  $\mathbf{B}$ . The Lagrangian of an ion is

$$L = \frac{Mv^2}{2} + \frac{Ze}{c} \mathbf{A} \cdot \mathbf{v} - Ze\phi, \quad (3)$$

where  $\mathbf{v}$  is the ion velocity,  $\mathbf{A}$  is the vector potential, and  $Ze\phi$  is the potential energy of the ion ( $\phi$  being the scalar potential). Choosing the vector potential acting on the  $i$ -th ion as

$A_i^\alpha = [\mathbf{B} \times \mathbf{u}_i]^\alpha / 2 = \varepsilon^{\alpha\beta\gamma} B^\beta u_i^\gamma / 2$  (where  $\mathbf{u}_i$  is the  $i$ -th ion displacement), the Lagrangian of the ion system can be written as:

$$\begin{aligned} L_B &= L_0 + \frac{Ze}{c} \sum_{i=1}^N A_i^\alpha \dot{u}_i^\alpha \\ &= L_0 + \frac{M\omega_B}{2} \sum_{i=1}^N \varepsilon^{\alpha\beta\gamma} \dot{u}_i^\alpha n^\beta u_i^\gamma . \end{aligned} \quad (4)$$

In this case,  $\mathbf{n}$  is the unit vector along the magnetic field,  $N$  is the total number of ions, and  $L_0$  is the field-free Lagrangian.

Introducing the same collective coordinates as at  $\mathbf{B} = 0$ ,

$$u_{lp}^\alpha = \sqrt{\frac{N_{\text{cell}}}{MN}} \sum_{\mathbf{k}} \mathcal{A}_{kp}^\alpha \exp(i\mathbf{k} \cdot \mathbf{R}_l) , \quad (5)$$

$$\mathcal{A}_{kp}^\alpha = \sqrt{\frac{MN_{\text{cell}}}{N}} \sum_l u_{lp}^\alpha \exp(-i\mathbf{k} \cdot \mathbf{R}_l) , \quad (6)$$

one can rearrange the Lagrangian as

$$L = L_0 + \frac{\omega_B}{2} \sum_{\mathbf{k}, p} \varepsilon^{\alpha\beta\gamma} \dot{\mathcal{A}}_{kp}^\alpha n^\beta \mathcal{A}_{-kp}^\gamma . \quad (7)$$

In this case,  $\mathbf{k}$  is a wavevector in the first Brillouin zone, index  $l$  enumerates direct lattice vectors  $\mathbf{R}_l$ ,  $N_{\text{cell}}$  is the number of ions in the primitive cell ( $N_{\text{cell}} = 1$  for simple lattices), and index  $p$  goes from 1 to  $N_{\text{cell}}$ . Summations in Eqs. (5) and (6) are over all wavevectors in the first Brillouin zone and over all direct lattice vectors, respectively. In the thermodynamic limit, with  $\mathcal{A}_{kp}^\alpha$  being interpreted as generalized coordinates of the system, one obtains the following Euler equation:

$$\ddot{\mathcal{A}}_{kp}^\alpha + \sum_{p'} \mathcal{D}_{pp'}^{\alpha\beta}(\mathbf{k}) \mathcal{A}_{kp'}^\beta + \omega_B \varepsilon^{\alpha\beta\gamma} n^\beta \dot{\mathcal{A}}_{kp}^\gamma = 0 , \quad (8)$$

where  $\mathcal{D}_{pp'}^{\alpha\beta}(\mathbf{k})$  is the dynamic matrix of the lattice at  $\mathbf{B} = 0$ . The Fourier-transform  $\mathcal{A}_{kp}^\alpha(t) \rightarrow A_{kp}^\alpha(\Omega)$  yields the algebraic equation

$$-\Omega^2 A_{kp}^\alpha + \sum_{p'} \mathcal{D}_{pp'}^{\alpha\beta}(\mathbf{k}) A_{kp'}^\beta - i\Omega\omega_B \varepsilon^{\alpha\beta\gamma} n^\beta A_{kp}^\gamma = 0 , \quad (9)$$

that can be solved if the ion vibration frequency  $\Omega$  satisfies the dispersion equation below [22]

$$\det \left\{ \mathcal{D}_{pp'}^{\alpha\beta} - \Omega^2 \delta_{pp'} \delta^{\alpha\beta} - i\Omega\omega_B \varepsilon^{\alpha\gamma\beta} n^\gamma \right\} = 0 . \quad (10)$$

Due to the presence of the third term on the left-hand side, Eq. (9) does not represent the eigennumber problem for a Hermitian matrix, and the respective polarization vectors are not orthogonal. This complicates the reduction of the Hamiltonian to the sum of Hamiltonians of independent oscillators. The proper procedure will be discussed in Sec. IV.

### III. PHONON SPECTRUM

There are  $3N_{\text{cell}}$  oscillation modes for a given vector  $\mathbf{k}$  in the first Brillouin zone. The frequencies of these modes satisfy the generalized Kohn's sum rule  $\sum_s \Omega_{\mathbf{k}s}^2 = N_{\text{cell}}(\omega_p^2 + \omega_B^2)$  [23].

At small  $k = |\mathbf{k}|$  the behavior of phonon frequencies is more complex than without the field. It depends substantially on the direction of  $\mathbf{k}$  with respect to  $\mathbf{B}$ . We restrict ourselves to  $N_{\text{cell}} = 1$ . It is possible to obtain the exact asymptotes of  $\Omega$  at small  $k$  (cf. Ref. [23]). In this limit, the dispersion equation (10) can be written as:

$$-\frac{\Omega^6}{\omega_p^6} + (1 + b^2) \frac{\Omega^4}{\omega_p^4} + E_B \frac{\Omega^2}{\omega_p^2} + F_0 = 0, \quad (11)$$

where

$$\begin{aligned} 16\pi E_B &= 16\pi E_0 - 16\pi b^2 (\hat{\mathbf{k}} \cdot \mathbf{n})^2 \\ &+ (ka_l)^2 b^2 [(\beta + \gamma_2) + (\alpha + 2\gamma_2) (\hat{\mathbf{k}} \cdot \mathbf{n})^2 \\ &+ (\gamma_1 - 3\gamma_2) (n_x^2 \hat{k}_x^2 + n_y^2 \hat{k}_y^2 + n_z^2 \hat{k}_z^2)], \end{aligned} \quad (12)$$

$\hat{\mathbf{k}} = \mathbf{k}/k$ , while the coefficients  $E_0$  and  $F_0$  are the same as in the field-free dispersion equation [26]:

$$\begin{aligned} 8\pi E_0 &= (ka_l)^2 [(\beta + \gamma_2) + (\gamma_1 - 3\gamma_2) (\hat{k}_x^2 \hat{k}_y^2 + \hat{k}_y^2 \hat{k}_z^2 + \hat{k}_z^2 \hat{k}_x^2)], \\ 256\pi^2 F_0 &= (ka_l)^4 [(\beta + \gamma_2)^2 + 2(\beta + \gamma_2)(\gamma_1 - 3\gamma_2) (\hat{k}_x^2 \hat{k}_y^2 + \hat{k}_y^2 \hat{k}_z^2 + \hat{k}_z^2 \hat{k}_x^2) \\ &+ 3(\gamma_1 - 3\gamma_2)^2 \hat{k}_x^2 \hat{k}_y^2 \hat{k}_z^2]. \end{aligned} \quad (13)$$

The constants  $\alpha$ ,  $\beta$ , and  $\gamma_{1,2}$  characterize the crystal at  $\mathbf{B} = 0$ . They were defined and calculated in Ref. [26], and were recalculated for bcc and fcc Coulomb lattices in Ref. [20]. They are reproduced in Table I, along with the lattice constant  $a_l$ , for completeness. The subscripts  $x$ ,  $y$ , and  $z$  refer to the Cartesian coordinate system aligned with the main cube of the respective reciprocal lattice.

The asymptote of the smallest frequency  $\Omega_1$  at  $k \rightarrow 0$  can be derived by dropping the  $\Omega^6$ -term and choosing the smallest root of the remaining quadratic equation:

$$\frac{\Omega_1^2}{\omega_p^2} = \frac{1}{2(1+b^2)} \left[ -E_B - \sqrt{E_B^2 - 4(1+b^2)F_0} \right]. \quad (14)$$

At sufficiently small  $k$ ,  $\Omega_1^2/\omega_p^2 \approx F_0/|E_B|$ . Then, for the phonons, propagating strictly perpendicular to the magnetic field,  $\Omega_1 \propto k$ , and the phonons are acoustic. If, on the other hand,  $\mathbf{k} \cdot \mathbf{n} \neq 0$ , then  $\Omega_1 \propto k^2$  at small  $k$ , in contrast with the linear dependence at  $\mathbf{B} = 0$ . As the angle between  $\mathbf{k}$  and  $\mathbf{B}$  decreases, the quadratic asymptote of  $\Omega_1$  becomes valid for wider range of  $k$ . Neglecting angular dependences and numerical factors in Eqs. (12) and (13), one can estimate the lowest phonon frequency as  $\Omega_1/\omega_p \sim ka_l/\sqrt{2+b^2}$  for propagation perpendicular to the field, and as  $\Omega_1/\omega_p \sim k^2 a_l^2/b$  for  $\mathbf{k} \cdot \mathbf{n} \neq 0$ . In both cases, at  $b \gg 1$ , the mode typical energy is inversely proportional to the field strength.

TABLE I: Dynamic matrix coefficients for bcc and fcc lattices

	$\alpha$	$\beta$	$\gamma_1$	$\gamma_2$	$na_l^3$
bcc	4.1243864	0.84911538	-3.4886939	-1.5915193	2
fcc	4.0036483	1.2376805	-4.2930041	-1.71184285	4

The asymptote of the biggest frequency  $\Omega_3$  can be found by dropping the last term in Eq. (11) and choosing the maximum root of the remaining quadratic equation:

$$\frac{\Omega_3^2}{\omega_p^2} = \frac{1}{2} \left[ 1 + b^2 + \sqrt{(1+b^2)^2 + 4E_B} \right]. \quad (15)$$

At small  $k$  this yields

$$\frac{\Omega_3^2}{\omega_p^2} = \frac{1}{2} \left[ 1 + b^2 + \sqrt{(1+b^2)^2 - 4b^2(\hat{\mathbf{k}} \cdot \mathbf{n})^2} \right] + O(k^2). \quad (16)$$

In general, at any  $\mathbf{k}$  and at  $b \gg 1$ , the biggest frequency  $\Omega_3 \approx \omega_B$ . This corresponds to the conventional cyclotron ion motion.

Consider  $k = 0$ . Then  $\Omega_3^2/\omega_p^2 = 1 + b^2$  for phonons propagating perpendicular to the field. From the sum rule, it follows that the intermediate frequency  $\Omega_2$  becomes 0 at  $k = 0$ . Because  $\Omega_2 > \Omega_1$ , it is clear that  $\Omega_2 \propto k$  for  $k \rightarrow 0$ . If, on the other hand, the phonon

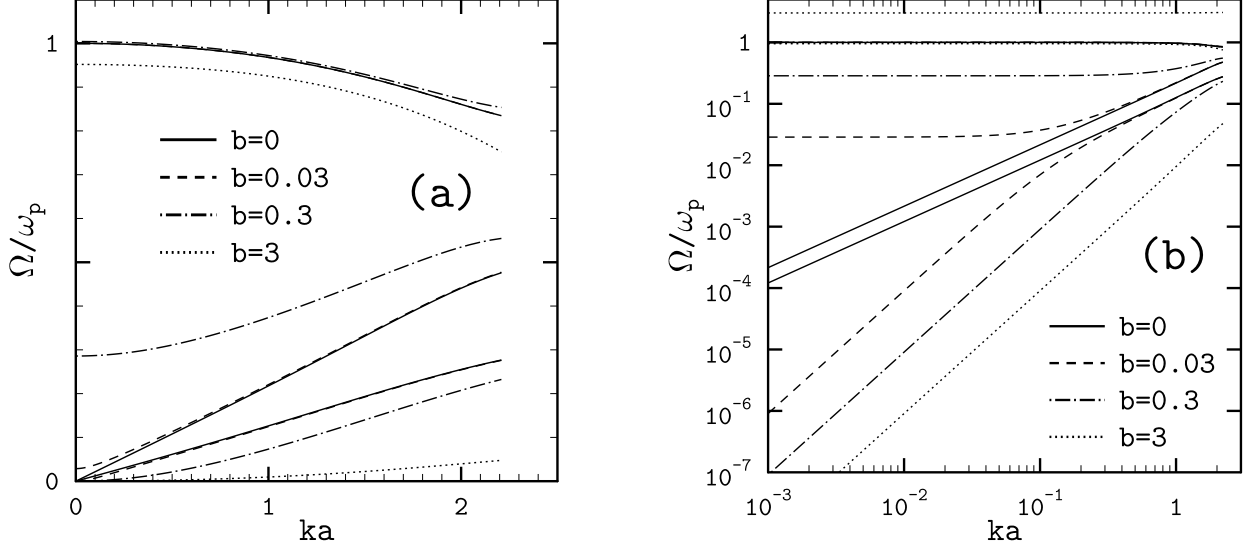


FIG. 1: Phonon spectrum of the magnetized bcc lattice for several values of  $b = \omega_B/\omega_p$  in natural (a) and logarithmic (b) scales. Slowly growing mode  $\Omega/\omega_p \approx 3$  at  $b = 3$  is not shown in panel (a). Magnetic field and wavevector  $\mathbf{k}$  orientations are defined in the text;  $a$  is the ion sphere radius.

propagates along the magnetic field, then at  $k = 0$  one has  $\Omega_3^2/\omega_p^2 = \max(1, b^2)$ , and, hence,  $\Omega_2^2/\omega_p^2 = \min(1, b^2)$ . Therefore both maximum and intermediate frequency modes are optical. As the angle between  $\mathbf{k}$  and  $\mathbf{B}$  decreases from  $\pi/2$  to 0, the value of  $\Omega_2$  at  $k \rightarrow 0$  increases from 0 to  $\min(\omega_p, \omega_B)$ , whereas the value of  $\Omega_3$  at  $k \rightarrow 0$  decreases from  $\sqrt{\omega_p^2 + \omega_B^2}$  to  $\max(\omega_p, \omega_B)$ .

Obviously, Eq. (11) can be solved analytically without neglecting any terms. However, at very small  $k$  analytical schemes become numerically unstable. The thermodynamic properties of Coulomb crystals at low temperatures require integration of functions containing the phonon frequencies near the center of the Brillouin zone. Under these conditions and especially at high magnetic fields the asymptotes given here become helpful.

Figure 1 shows the phonon spectrum of the bcc lattice (in natural and logarithmic scales) in the direction of  $\mathbf{k}$  determined by the polar angle  $\theta = 1.3 \tan^{-1} \sqrt{2}$  and the azimuthal angle  $\phi = 0.9\pi/4$  [angles  $\theta$  and  $\phi$  are defined with respect to the same Cartesian reference frame as the  $x, y, z$ -subscripts in Eqs. (12) and (13)]. The magnetic field is parallel to the direction from an ion towards one of its nearest neighbors ( $\theta = \tan^{-1} \sqrt{2}$ ,  $\phi = \pi/4$ ). For  $ka \lesssim 0.01$ , analytic asymptotes discussed above are used; at higher  $ka$ , exact calculations are performed. One can observe the quadratic dependence of the lowest frequency on  $k$

near the Brillouin zone center. The dependence becomes linear closer to the Brillouin zone boundary (at  $b \ll 1$ ).

The polarization of the electron background in the absence of the magnetic field converts the optical mode with a frequency  $\approx \omega_p$  into an acoustic mode in the vicinity of the Brillouin zone center (e.g., [25, 27]). The background polarization effects in a magnetized crystal will be investigated elsewhere. A similar conversion effect can be expected in this case as well, except that one of the modes must remain optical close to the center of the zone, with a frequency  $\Omega \approx \omega_B$ . This is so, because the coefficient of the  $\Omega^4$ -term in the dispersion equation (10), that determines the sum of the squares of all frequencies, will continue to contain  $\omega_B^2$ , whereas in the field-free case at  $k \rightarrow 0$  the  $\Omega^4$ -term tends to zero for polarizable background.

#### IV. HAMILTONIAN OF THE COULOMB CRYSTAL IN THE MAGNETIC FIELD

In this section the Hamiltonian of the Coulomb crystal in the magnetic field is represented as a sum of Hamiltonians of independent oscillators. The derivation follows that of Ref. [22], but some additional details are provided. Consider the Cartesian reference frame with the axes directed along the eigenvectors of the matrix  $\mathcal{D}^{\alpha\beta}(\mathbf{k})$  (again  $N_{\text{cell}} = 1$ ). Then the Lagrangian (7) has the form

$$L_B = \frac{1}{2} \sum_{\mathbf{k}} \dot{\mathcal{A}}_{\mathbf{k}}^{\alpha} \dot{\mathcal{A}}_{-\mathbf{k}}^{\alpha} - U_0 - \frac{1}{2} \sum_{\mathbf{k}} \omega_{\mathbf{k}\alpha}^2 \mathcal{A}_{\mathbf{k}}^{\alpha} \mathcal{A}_{-\mathbf{k}}^{\alpha} + \frac{\omega_B}{2} \sum_{\mathbf{k}} \varepsilon^{\alpha\beta\gamma} \dot{\mathcal{A}}_{\mathbf{k}}^{\alpha} n^{\beta} \mathcal{A}_{-\mathbf{k}}^{\gamma}. \quad (17)$$

In this case,  $\omega_{\mathbf{k}\alpha}$  is the phonon frequency at  $\mathbf{B} = 0$ . Omitting the constant equilibrium electrostatic energy term  $U_0$  and turning to the Hamiltonian  $H_B$ , one has

$$\mathcal{P}_{\mathbf{k}}^{\alpha} = \dot{\mathcal{A}}_{-\mathbf{k}}^{\alpha} + \frac{\omega_B}{2} \varepsilon^{\alpha\beta\gamma} n^{\beta} \mathcal{A}_{-\mathbf{k}}^{\gamma}, \quad (18)$$

$$H_B = \sum_{\mathbf{k}} \dot{\mathcal{A}}_{\mathbf{k}}^{\alpha} \mathcal{P}_{\mathbf{k}}^{\alpha} - L_B = \frac{1}{2} \sum_{\mathbf{k}} \pi_{-\mathbf{k}}^{\alpha} \pi_{\mathbf{k}}^{\alpha} + \frac{1}{2} \sum_{\mathbf{k}} \omega_{\mathbf{k}\alpha}^2 \mathcal{A}_{\mathbf{k}}^{\alpha} \mathcal{A}_{-\mathbf{k}}^{\alpha}, \quad (19)$$

where  $\pi_{\mathbf{k}}^{\alpha} = \mathcal{P}_{\mathbf{k}}^{\alpha} - \omega_B \varepsilon^{\alpha\beta\gamma} n^{\beta} \mathcal{A}_{-\mathbf{k}}^{\gamma}/2$ . In the quantum formalism,  $\mathcal{A}_{\mathbf{k}}^{\alpha}$  and  $\mathcal{P}_{\mathbf{k}}^{\alpha}$  become operators with the usual commutation rules  $[\mathcal{A}_{\mathbf{k}}^{\alpha}, \mathcal{P}_{\mathbf{k}'}^{\beta}] = i\hbar \delta^{\alpha\beta} \delta_{\mathbf{k}\mathbf{k}'}$ . However, the operators  $\pi_{\mathbf{k}}^{\alpha}$  and

$\pi_{-\mathbf{k}}^\beta$  do not commute at  $\alpha \neq \beta$ :  $[\pi_{\mathbf{k}}^\alpha, \pi_{\mathbf{k}'}^\beta] = i\hbar\omega_B \varepsilon^{\beta\gamma\alpha} n^\gamma \delta_{\mathbf{k}', -\mathbf{k}}$ . Consequently, the creation and annihilation operators, defined in the same way as at  $\mathbf{B} = 0$ , but with  $\pi_{\mathbf{k}}^\alpha$  in place of  $\mathcal{P}_{\mathbf{k}}^\alpha$ , do not satisfy the required commutation relationships.

In this situation one constructs the creation and annihilation operators as linear combinations of the operators of generalized coordinates and momenta (e.g., Ref. [22]),

$$\hat{a}_{\mathbf{k}}^\dagger = \alpha_{\mathbf{k}}^\lambda \pi_{\mathbf{k}}^\lambda + \beta_{\mathbf{k}}^\lambda \mathcal{A}_{-\mathbf{k}}^\lambda, \quad (20)$$

where  $\alpha_{\mathbf{k}}^\lambda$  and  $\beta_{\mathbf{k}}^\lambda$  are constant coefficients (and summation over  $\lambda$  is implied). They can be determined from the equation  $[H_B, \hat{a}_{\mathbf{k}}^\dagger] = \hbar\Omega_{\mathbf{k}} \hat{a}_{\mathbf{k}}^\dagger$  (e.g., Ref. [22]). Using Eqs. (19) and (20), one arrives at

$$\begin{aligned} \hbar\Omega_{\mathbf{k}} (\alpha_{\mathbf{k}}^\lambda \pi_{\mathbf{k}}^\lambda + \beta_{\mathbf{k}}^\lambda \mathcal{A}_{-\mathbf{k}}^\lambda) &= i\hbar\omega_B \varepsilon^{\lambda\gamma\alpha} n^\gamma \alpha_{\mathbf{k}}^\lambda \pi_{\mathbf{k}}^\alpha \\ &+ i\hbar\omega_{\mathbf{k}\lambda}^2 \alpha_{\mathbf{k}}^\lambda \mathcal{A}_{-\mathbf{k}}^\lambda - i\hbar\beta_{\mathbf{k}}^\lambda \pi_{\mathbf{k}}^\lambda, \end{aligned} \quad (21)$$

or

$$\Omega_{\mathbf{k}} \beta_{\mathbf{k}}^\lambda = i\omega_{\mathbf{k}\lambda}^2 \alpha_{\mathbf{k}}^\lambda, \quad (22)$$

$$\Omega_{\mathbf{k}} \alpha_{\mathbf{k}}^\lambda = i\omega_B \varepsilon^{\alpha\gamma\lambda} n^\gamma \alpha_{\mathbf{k}}^\alpha - i\beta_{\mathbf{k}}^\lambda, \quad (23)$$

so that

$$(\omega_{\mathbf{k}\lambda}^2 - \Omega_{\mathbf{k}}^2) \alpha_{\mathbf{k}}^\lambda - i\Omega_{\mathbf{k}} \omega_B \varepsilon^{\lambda\gamma\alpha} n^\gamma \alpha_{\mathbf{k}}^\alpha = 0. \quad (24)$$

The system (24) can be solved only if the quantities  $\Omega_{\mathbf{k}}$  satisfy the dispersion equation (10), i.e., if they are the eigenfrequencies of the oscillation modes with the wavevector  $\mathbf{k}$ . Therefore, there are three possible solutions for the operator  $\hat{a}_{\mathbf{k}}^\dagger$ , corresponding to the three generally different frequencies  $\Omega_{\mathbf{k}s}$ ,  $s = 1, 2, 3$ :  $\hat{a}_{\mathbf{k}s}^\dagger = \alpha_{\mathbf{k}s}^\lambda (\pi_{\mathbf{k}}^\lambda + i\omega_{\mathbf{k}\lambda}^2 \mathcal{A}_{-\mathbf{k}}^\lambda / \Omega_{\mathbf{k}s})$ . Evidently, the equations for the coefficients  $\alpha_{\mathbf{k}s}^\lambda$  and  $\alpha_{-\mathbf{k}s}^\lambda$  coincide. Thus from now on index  $\mathbf{k}$  will be omitted where possible.

The solutions of the system (24) are sets of the cofactors to any of the rows of the matrix [22]

$$\left\| \begin{array}{ccc} \omega_x^2 - \Omega_s^2 & i\Omega_s \omega_B n^z & -i\Omega_s \omega_B n^y \\ -i\Omega_s \omega_B n^z & \omega_y^2 - \Omega_s^2 & i\Omega_s \omega_B n^x \\ i\Omega_s \omega_B n^y & -i\Omega_s \omega_B n^x & \omega_z^2 - \Omega_s^2 \end{array} \right\| \quad (25)$$

(these sets are proportional to each other). Now one has to normalize these solutions together with the operators  $a_s^\dagger$ , so that  $[\hat{a}_s, \hat{a}_s^\dagger] = 1$ . Accordingly,

$$\begin{aligned} [\hat{a}_s, \hat{a}_{s'}^\dagger] &= \alpha_s^{\lambda*} \alpha_{s'}^{\lambda'} i\hbar\omega_B \varepsilon^{\lambda'\gamma\lambda} n^\gamma \\ &\quad + \alpha_s^{\lambda*} \alpha_{s'}^\lambda \hbar\omega_\lambda^2 \left( \frac{1}{\Omega_s} + \frac{1}{\Omega_{s'}} \right) \\ &= \alpha_s^{\lambda*} \alpha_{s'}^\lambda \hbar \left( \frac{\omega_\lambda^2}{\Omega_s} + \Omega_{s'} \right), \end{aligned} \quad (26)$$

where Eq. (24) was employed. Now consider the following sequence of equations,

$$\begin{aligned} 0 &= \alpha_{s'}^\lambda [(\Omega_s^2 - \omega_\lambda^2) \alpha_s^{\lambda*} - i\Omega_s \omega_B \varepsilon^{\lambda\nu\gamma} n^\gamma \alpha_s^{\nu*}] \\ &= \alpha_{s'}^\lambda \alpha_s^{\lambda*} (\Omega_s^2 - \omega_\lambda^2) + \alpha_{s'}^\nu \alpha_s^{\nu*} \frac{\Omega_s}{\Omega_{s'}} (\omega_\nu^2 - \Omega_{s'}^2) \\ &= \alpha_{s'}^\lambda \alpha_s^{\lambda*} \left( \frac{\Omega_s}{\Omega_{s'}} - 1 \right) (\omega_\lambda^2 + \Omega_s \Omega_{s'}) \end{aligned} \quad (27)$$

[where Eq. (24) was used twice]. Thus the right-hand side of Eq. (26) vanishes, if  $\Omega_s \neq \Omega_{s'}$ .

This property is analogous to the orthogonality condition for the polarization vectors at  $\mathbf{B} = 0$ . At  $s = s'$ , Eq. (26) determines the normalization of the coefficients  $\alpha_s^\lambda$ :

$$\alpha_s^\lambda \alpha_s^{\lambda*} \hbar \left( \frac{\omega_\lambda^2}{\Omega_s} + \Omega_s \right) = 1. \quad (28)$$

All the other commutators of the operators  $\hat{a}_s$  and  $\hat{a}_s^\dagger$  vanish automatically.

Owing to the equality  $[H_B, \hat{a}^\dagger] = \hbar\Omega\hat{a}^\dagger$  and the normalization relationships obtained above, the Hamiltonian (19) can be rewritten in the canonical form

$$H_B = \sum_{\mathbf{k}s} \hbar\Omega_{\mathbf{k}s} \left( \hat{a}_{\mathbf{k}s}^\dagger \hat{a}_{\mathbf{k}s} + \frac{1}{2} \right). \quad (29)$$

Moreover, with the help of Eqs. (19) and (20), it is possible to prove the relationships:

$$\sum_s \alpha_s^\lambda \alpha_s^{\lambda'*} - \alpha_s^{\lambda*} \alpha_s^{\lambda'} = 0, \quad (30)$$

$$\hbar \sum_s \frac{\omega_\lambda \omega_{\lambda'}}{\Omega_s} (\alpha_s^\lambda \alpha_s^{\lambda'*} + \alpha_s^{\lambda*} \alpha_s^{\lambda'}) = \delta^{\lambda\lambda'}, \quad (31)$$

$$\hbar \sum_s \Omega_s (\alpha_s^\lambda \alpha_s^{\lambda'*} + \alpha_s^{\lambda*} \alpha_s^{\lambda'}) = \delta^{\lambda\lambda'}. \quad (32)$$

Multiplying  $\hat{a}_{-\mathbf{k}s}^\dagger$  by  $\alpha_{\mathbf{k}s}^{\lambda*}$ , and  $\hat{a}_{\mathbf{k}s}$  by  $\alpha_{\mathbf{k}s}^\lambda$ , summing over  $s$ , subtracting the second expression from the first one, and also using (30) and (31), one obtains

$$\mathcal{A}_{\mathbf{k}}^\lambda = -i\hbar \sum_s \alpha_{\mathbf{k}s}^{\lambda*} \hat{a}_{-\mathbf{k}s}^\dagger + i\alpha_{\mathbf{k}s}^\lambda \hat{a}_{\mathbf{k}s}. \quad (33)$$

The above formula is instrumental in calculations of such crystal properties as the Debye-Waller factor and the rms ion displacement from a lattice site in the magnetic field. These results are reported in Sec. VII.

## V. PHONON THERMODYNAMIC FUNCTIONS OF THE MAGNETIZED COULOMB CRYSTAL

Phonon thermodynamic functions in the magnetic field are calculated using the same general formulas (e.g., [28]) and numerical integration schemes (e.g., [6, 20, 29]) as in the field-free case. The phonon free energy (with phonon chemical potential  $\mu = 0$  and neglecting zero-point contribution) reads

$$\begin{aligned} F &= T \sum_{\mathbf{k}s} \ln \left[ 1 - \exp \left( -\frac{\hbar \Omega_{\mathbf{k}s}}{T} \right) \right] \\ &= V \sum_s \int_{\text{BZ}} \frac{d\mathbf{k}}{(2\pi)^3} \ln \left[ 1 - \exp \left( -\frac{\hbar \Omega_{\mathbf{k}s}}{T} \right) \right], \end{aligned} \quad (34)$$

where  $V$  is the volume, and the integral is over the first Brillouin zone. The phonon thermal energy  $E$  and heat capacity  $C$  are then given by

$$E = F - T \left( \frac{\partial F}{\partial T} \right)_{\mu, V} = \sum_{\mathbf{k}s} \frac{\hbar \Omega_{\mathbf{k}s}}{e^{\hbar \Omega_{\mathbf{k}s}/T} - 1} \quad (35)$$

$$C = -T \left( \frac{\partial^2 F}{\partial T^2} \right)_{\mu, V} = \frac{1}{4T^2} \sum_{\mathbf{k}s} \frac{\hbar^2 \Omega_{\mathbf{k}s}^2}{\sinh^2(\hbar \Omega_{\mathbf{k}s}/2T)}. \quad (36)$$

In the magnetic field, there are two new parameters,  $b = \omega_B/\omega_p$  and the field direction. A study of frequency moments of the phonon spectrum in Sec. VIII will show that the dependence of these moments on the field direction is rather weak. This allows one to expect that the dependence of thermodynamic functions on the field direction is also weak. Thus, in the present section the consideration is restricted to the field direction, which corresponds to the minimum zero-point energy of the crystal. For the bcc lattice, it is the direction from a lattice site to one of its closest neighbors.

The calculated phonon heat capacity per one ion is presented in Fig. 2 in logarithmic and linear scales [panels (a) and (b), respectively] as a function of  $\theta^{-1} = T/T_p$  for several values of  $b$ . In Fig. 2(a) one can clearly see the change of the low-temperature asymptote from  $T^3$  to  $T^{3/2}$  due to the appearance of the soft mode  $\Omega \propto k^2$  for non-zero  $B$ . Also, this easily

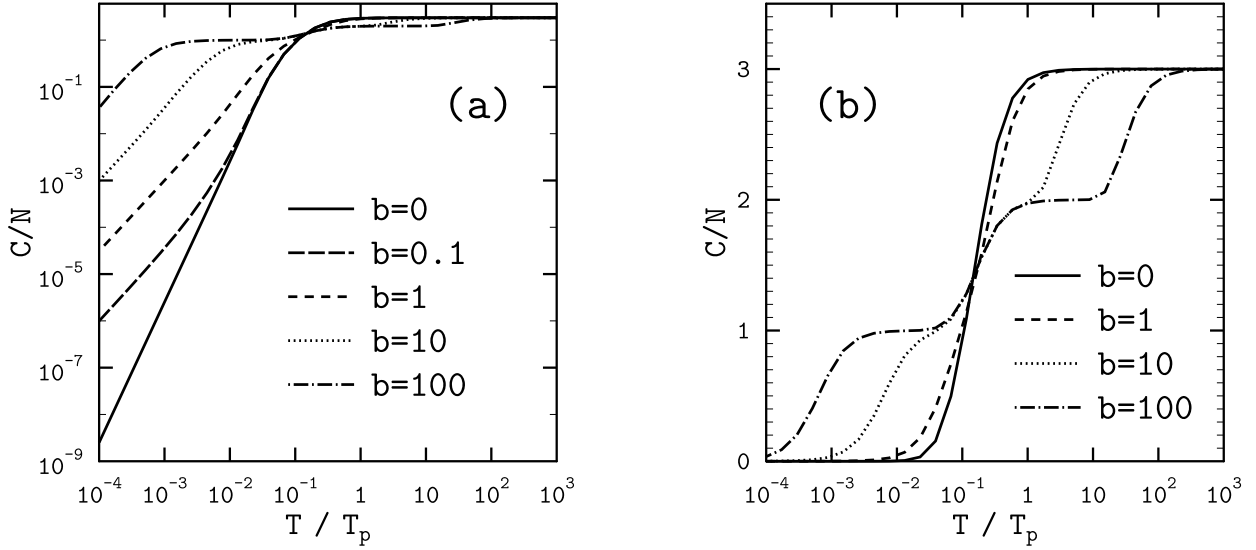


FIG. 2: Phonon specific heat (per ion) for the bcc lattice as a function of temperature for several values of the magnetic field in logarithmic (a) and linear (b) scales. The magnetic field is directed towards one of the nearest neighbors.

excited mode (e.g., at  $b = 100$ ) is responsible for a relatively high specific heat  $C/N \sim 1$  all the way up to  $\theta \sim 10^3$ . At these temperatures the field-free specific heat is already down by 6 orders of magnitude.

In strong magnetic fields, higher temperatures are required to achieve the classical regime as compared to the field-free case. This is so, because the classical regime occurs when many phonons are excited in *all* modes. In a strong magnetic field, there is the high-frequency (cyclotron) mode,  $\Omega_3 \approx \omega_B$  (Sec. III). Hence, the classical regime is realized if  $b\theta \ll 1$ , in contrast to the conventional criterion  $\theta \ll 1$  at  $B = 0$ . This is illustrated in Fig. 2(b). For instance, for  $b = 100$  the classical value  $C/N = 3$  is reached only at  $\theta \lesssim 0.01$ .

The energies of three phonon modes are spaced far away from each other in strong magnetic fields. The minimum frequency  $\Omega_1 \propto 1/B$ , the maximum frequency  $\Omega_3 \approx \omega_B$ , and the intermediate frequency  $\Omega_2 \sim \omega_p$  (Sec. III). This gives rise to the pronounced staircase structure of the heat capacity seen in Fig. 2(b) at  $b = 10$  and 100.

This discussion is further illustrated by Fig. 3, where one can assess qualitatively the behavior of the specific heat in various domains of the  $T$ - $B$  plane. At high temperatures, the crystal is classic and the specific heat reaches its maximum value of 3. In strong magnetic fields ( $b \gg 1$ ) when the temperature drops below  $\hbar\omega_B$ , the cyclotron phonon mode is frozen

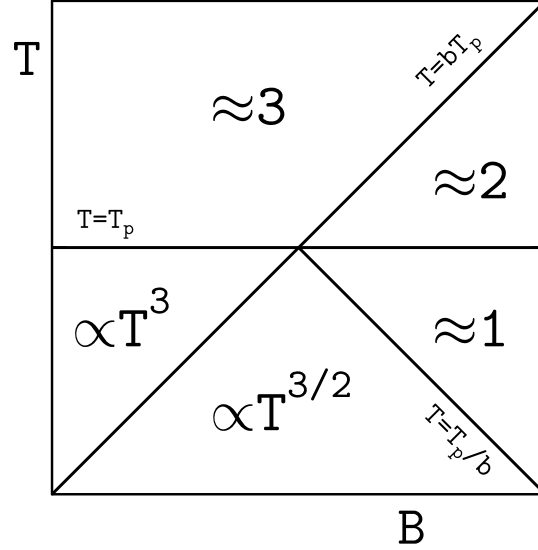


FIG. 3: A sketch of the specific heat behavior in various domains of the  $T$ - $B$  plane. The point, where all straight lines cross, corresponds to  $b = \theta = 1$ .

out and  $C/N \approx 2$ . As the temperature drops further, below  $T_p$ , the intermediate mode  $\Omega_2$  freezes out in large portions of the Brillouin zone, and the specific heat, now mainly due to the fully-excited soft mode, approaches 1. By contrast, in a non-magnetized ( $b \ll 1$ ) crystal, the two lower modes deviate from being acoustic only in the very vicinity of the Brillouin zone center, while the third one is  $\approx \omega_p$ . Hence, when  $T$  drops below  $T_p$  in such a crystal, the Debye law  $C \propto T^3$  is recovered. Finally, at any  $b$ , when the temperature is so low, that only the least energetic mode contains any heat and the  $\Omega \propto k^2$  law is probed,  $C \propto T^{3/2}$  behavior results.

In Fig. 4 phonon thermal energy and entropy  $S = (E - F)/T$  are plotted. In the case of energy, plotted in the linear scale in Fig. 4(a), one observes again the staircase structure. Though less pronounced, it occurs for the same reason as for the specific heat. The classical harmonic oscillator limit  $E = 3NT$  is naturally reproduced. At low temperatures, the magnetic field gives rise to the  $T^2$  dependence of the energy instead of the  $T^4$  field-free asymptote. For sufficiently low temperatures, the thermal energy is dominated by the zero-point energy, determined by the spectrum moment  $u_1$  and discussed in Sec. VIII. The numerical calculations of the entropy are shown in Fig. 4(b). In this case, as for the specific heat, the familiar field-free  $T^3$  asymptote is replaced by  $T^{3/2}$  in the quantum magnetized crystal. In the classical regime, the entropy depends on temperature logarithmically and is

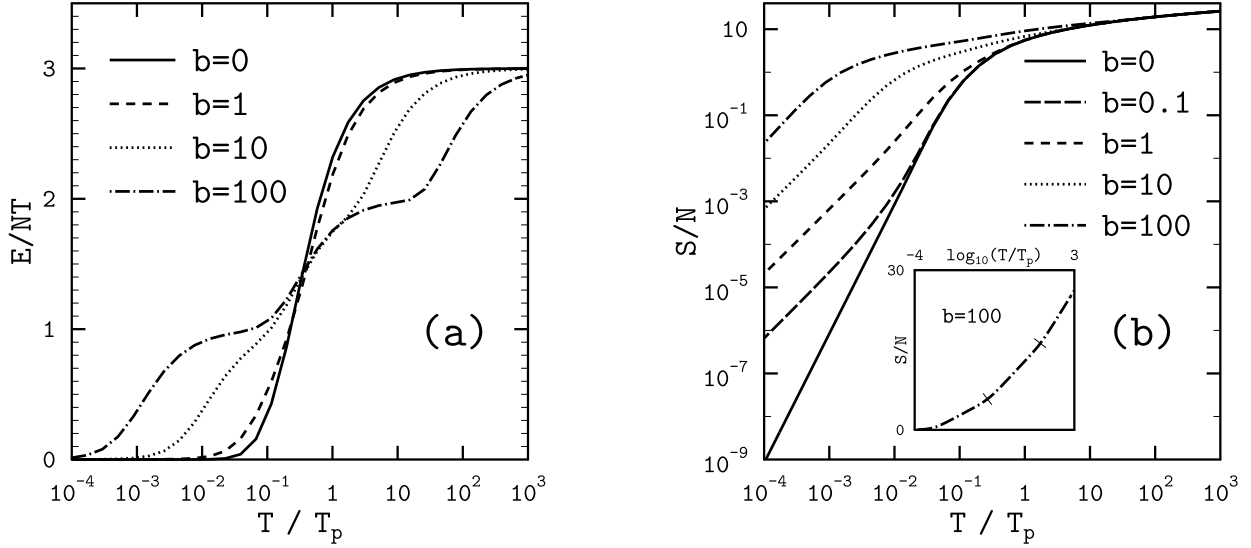


FIG. 4: Phonon energy per ion divided by  $T$  (a) and phonon entropy per ion (b) for the bcc lattice as functions of temperature for several values of the magnetic field. Inset in panel (b) shows  $S/N$  in the linear scale at  $b = 100$ . The magnetic field is directed towards one of the nearest neighbors.

insensitive to the magnetic field. This asymptote is discussed in some detail in Sec. VIII. When drawn in linear scale, the entropy, as a function of  $\log_{10} T$ , also shows an atypical structure at  $b \gg 1$  [inset in Fig. 4(b)]. In this case, the dependence becomes piece-wise linear with several slope changes, corresponding to the sequential excitation of the three phonon modes.

Clearly, magnetized crystal thermodynamics, constructed in this Section, cannot be described by the well-known in solid state physics Debye model (e.g., [28]). On the other hand, at  $b \gg 1$ , partial thermodynamic quantities due to the cyclotron mode  $\Omega_3$ , can be represented with high accuracy by the simple Einstein model (e.g., [30]).

## VI. APPLICATION TO MAGNETAR CRUST

As a practical application of the previous section results, consider fully ionized iron plasma in neutron star crust (Sec. I). Typical values of  $\theta$  and  $b$  at  $B = 10^{15}$  and  $10^{16}$  G can be estimated from Fig. 5. The curve  $\Gamma = 175$  shows the melting line of the classical Coulomb crystal at  $B = 0$ . The line  $T = Z^2 e^2 / a$  represents typical electrostatic energy per ion (and separates the regions of a free ion gas above the line, and a strongly coupled ion system

below the line). The electron degeneracy temperature is shown by dotted lines marked  $T_{F0}$ ,  $T_{F15}$ , and  $T_{F16}$  for three values of the magnetic field,  $B = 0$ ,  $10^{15}$ , and  $10^{16}$  G, respectively. Finally,  $E_{Z15}$  and  $E_{Z16}$  are the electron ground-state energies of one-electron iron ion for  $B = 10^{15}$  or  $10^{16}$  G, respectively. These energies are calculated using rescaling of equivalent hydrogen energies  $E(Z, B) = Z^2 E(Z = 1, B/Z^2)$  (e.g., [31]), and the fitting formula [32] for the energy of the  $s = 0$  state in the hydrogen atom. The assumption of full ionization in the degenerate plasma can be used if  $T_F > E_Z$  (for a given magnetic field). At  $T_F \gg E_Z$ , the electron gas is nearly incompressible, and the rigid electron background model is very well justified. At  $T_F \lesssim E_Z$  the plasma cannot be treated as fully ionized, but even in this case one can use present results for estimates by employing the effective ion charge approximation.

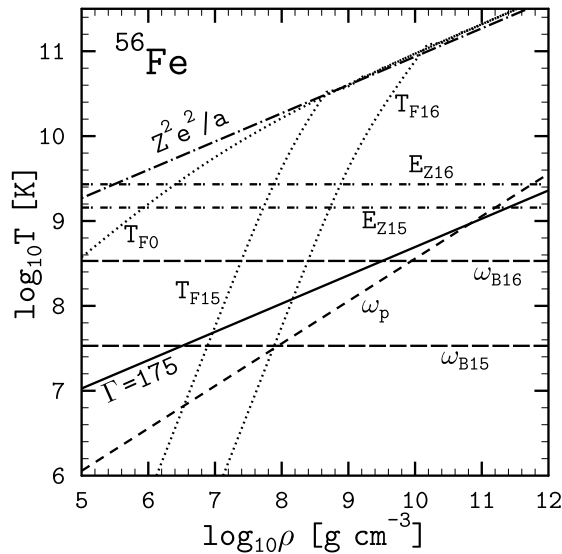


FIG. 5: Temperature-density diagram for fully ionized  $^{56}\text{Fe}$  matter.  $\Gamma = 175$  is the classical crystal melting line.  $T_F$  and  $E_Z$  mark electron degeneracy temperature and electron-ion binding energy (see text for details). Subscripts 0, 15, and 16 refer to the magnetic field values  $B = 0$ ,  $10^{15}$ , and  $10^{16}$  G, respectively. Note, that  $E_{Z0} = 1.1 \times 10^8$  K.

Figure 6 demonstrates the phonon and electron specific heat (per ion) of fully ionized  $^{56}\text{Fe}$  plasma as a function of density (a) and temperature (b) at  $B = 0$  and  $2 \times 10^{15}$  G. The electron contribution is calculated using standard formulas for strongly degenerate relativistic Fermi gas. For  $B = 2 \times 10^{15}$  G under the displayed conditions the plasma electrons fill the lowest Landau level only; the next Landau level would be occupied at  $\rho \gtrsim 10^9$  g cm $^{-3}$ , and the plasma would become partly ionized at  $\rho \lesssim 10^8$  g cm $^{-3}$  (cf. Fig. 5). The temperature

dependence of the electron specific heat is linear, and near coincidence of two electron lines in Fig. 6(b) is largely accidental. For the ions to crystallize, the temperature must be below the melting temperature, which is  $\sim 10^8$  K in the density range considered (cf. Fig. 5).

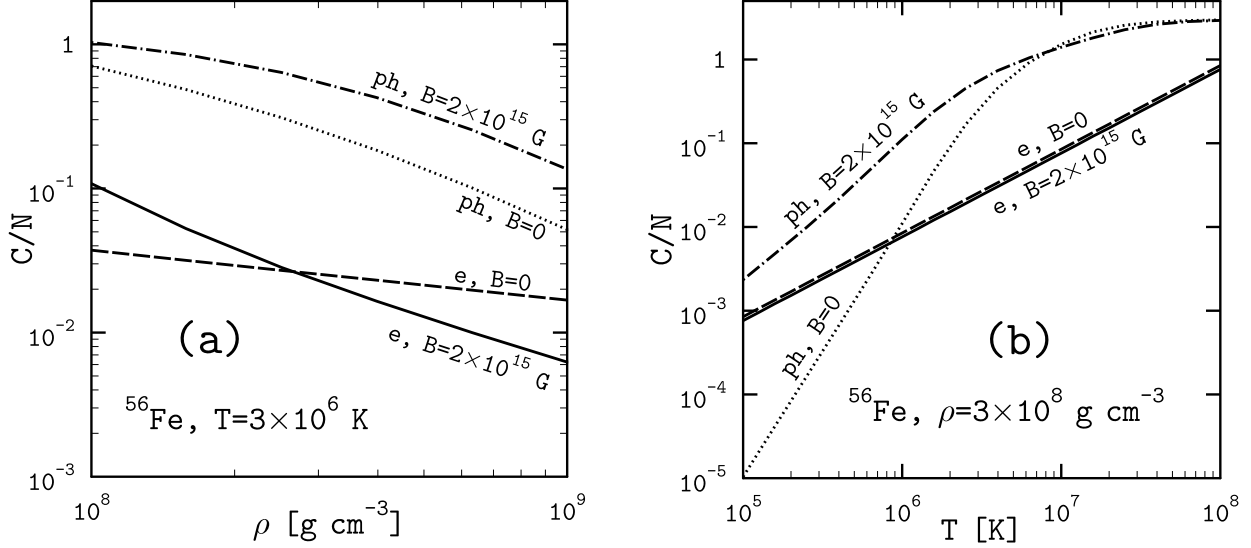


FIG. 6: Phonon and electron specific heat (per ion) of fully ionized  $^{56}\text{Fe}$  matter versus density (a) and temperature (b) at  $B = 0$  and  $2 \times 10^{15}$  G. For the  $B \neq 0$  case,  $b\theta = 23$  in panel (a);  $T_p = 6.2 \times 10^7$  K and  $b = 1.09$  in panel (b).

The phonon contribution at  $B = 0$ , recalculated here, reproduces the results of [6]. At  $B = 2 \times 10^{15}$  G the results of the present work are plotted. As seen from Fig. 6, phonons dominate electrons in the specific heat in a wide range of temperatures and densities. The magnetic field provides an extra boost to the phonon specific heat, especially at lower temperatures (in the quantum regime) due to the easily excited soft mode.

## VII. ION VIBRATIONS AND THE DEBYE-WALLER FACTOR IN THE MAGNETIZED CRYSTAL

Using Eqs. (5) and (33), one can derive the expression for the operator of the ion displacement from its equilibrium lattice position:

$$\hat{u}_1^\lambda = \frac{i\hbar}{\sqrt{MN}} \sum_{\mathbf{k}s} (\alpha_{\mathbf{k}s}^\lambda \hat{a}_{\mathbf{k}s} - \alpha_{\mathbf{k}s}^{\lambda*} \hat{a}_{-\mathbf{k}s}^\dagger) \exp(i\mathbf{k} \cdot \mathbf{R}_l). \quad (37)$$

Then the rms ion displacement  $r_T = \sqrt{\langle \hat{u}^\lambda \hat{u}^\lambda \rangle_T}$  can be calculated as

$$\begin{aligned} \frac{r_T^2}{a^2} &= \frac{\hbar^2}{MN a^2} \sum_{\mathbf{k}s} \alpha_{\mathbf{k}s}^{\lambda*} \alpha_{\mathbf{k}s}^\lambda \langle \hat{a}_{\mathbf{k}s}^\dagger \hat{a}_{\mathbf{k}s} + \hat{a}_{\mathbf{k}s} \hat{a}_{\mathbf{k}s}^\dagger \rangle_T \\ &= \frac{\theta}{3N\Gamma} \sum_{\mathbf{k}s} (\hbar\omega_p \alpha_{\mathbf{k}s}^{\lambda*} \alpha_{\mathbf{k}s}^\lambda) (2\bar{n}_{\mathbf{k}s} + 1) \equiv \frac{\theta}{\Gamma} \mathcal{F}(\theta, b) \end{aligned} \quad (38)$$

[cf. Eq. (28)], where  $\bar{n}_{\mathbf{k}s} = (e^{\hbar\Omega_{\mathbf{k}s}/T} - 1)^{-1}$  is the mean number of phonons in a mode  $\mathbf{k}s$ . In addition, it is possible to find the rms ion displacement  $u_{\hat{\mathbf{q}}}$  in the direction along an arbitrary unit vector  $\hat{\mathbf{q}}$ ,

$$\begin{aligned} u_{\hat{\mathbf{q}}}^2 &= \langle \hat{u}^\lambda \hat{u}^\mu \hat{q}^\lambda \hat{q}^\mu \rangle_T \\ &= \frac{\hbar^2}{MN} \sum_{\mathbf{k}s} \alpha_{\mathbf{k}s}^{\lambda*} \alpha_{\mathbf{k}s}^\mu \hat{q}^\lambda \hat{q}^\mu (2\bar{n}_{\mathbf{k}s} + 1). \end{aligned} \quad (39)$$

In the field-free case,  $u_{\hat{\mathbf{q}}}$  is isotropic (in the bcc crystal), but in the magnetic field it becomes anisotropic.

Amplitudes of ion oscillations are depicted in Fig. 7. The ion equilibrium position is at the origin. The  $Y$ -axis is parallel to  $\mathbf{B}$  and to the direction towards one of the nearest neighbors. There is symmetry in the plane azimuthal with respect to  $\mathbf{B}$  (the plane perpendicular to the  $Y$ -axis). Hence, the  $X$ -axis indicates an arbitrary direction orthogonal to  $\mathbf{B}$ . The distance between the origin and a point on a chosen curve is equal to the rms displacement  $u_{\hat{\mathbf{q}}}$  in the given direction. The distance is expressed in units of the spacing between the nearest neighbors,  $a_n = a_l \sqrt{3}/2 = (3\pi^2)^{1/6} a$  (for bcc lattice). Solid, dash-dotted, long-dashed, dotted, and short-dashed curves correspond to  $b = 100, 10, 1, 0.1$ , and  $0.01$ , respectively. The 6 panels of Fig. 7 are for the 6 values of the quantum parameter  $\theta$ , from  $0.1$  to  $10^4$ . The ion displacement at a different  $\Gamma$  (for given  $\theta$  and  $b$ ) can be found by straightforward scaling per Eq. (38).

The quantity  $u_{\hat{\mathbf{q}}}$  is related to the Debye-Waller factor  $W(\hat{\mathbf{q}})$ :  $\langle \exp(i\hat{\mathbf{q}} \cdot \hat{\mathbf{u}}) \rangle_T = \exp(-W)$ . The thermal averaging yields

$$\langle \exp(i\hat{\mathbf{q}} \cdot \hat{\mathbf{u}}) \rangle_T = \exp \left[ -\frac{\hbar^2}{MN} \sum_{\mathbf{k}s} \hat{q}^\lambda \hat{q}^\mu \alpha_{\mathbf{k}s}^{\lambda*} \alpha_{\mathbf{k}s}^\mu \left( \bar{n}_{\mathbf{k}s} + \frac{1}{2} \right) \right].$$

Thus,  $u_{\hat{\mathbf{q}}}^2 = 2W(\hat{\mathbf{q}})$ .

As shown in Fig. 7, the ion displacements at  $\theta \lesssim 1$  are insensitive to the magnetic field (all 5 lines merge) and isotropic. At  $\theta \sim 10$  the displacement along the field remains essentially

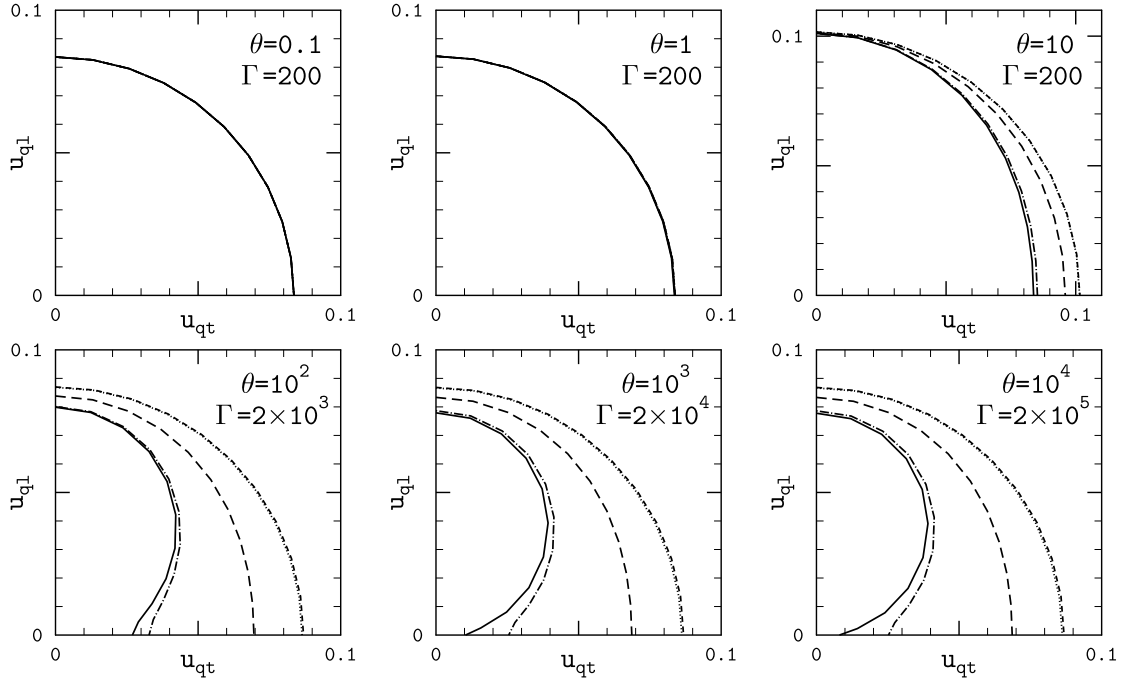


FIG. 7: The rms ion displacement from the equilibrium position (the origin).  $Y$ -axis ( $u_{ql}$ ) is parallel,  $X$ -axis ( $u_{qt}$ ) is perpendicular to  $\mathbf{B}$ .  $u_{ql}$  and  $u_{qt}$  are in units of the distance to the nearest neighbor. The solid, dash-dotted, long-dashed, dotted, and short-dashed curves correspond to  $b = 100, 10, 1, 0.1$ , and  $0.01$ , respectively. The distance between the origin and a point on a chosen curve is equal to the rms ion displacement  $u_{\hat{q}}$  in that direction.

the same as at  $B = 0$ , whereas the transverse displacements shrink. The net effect will be an increase of the crystal stability and melting temperature. The anisotropy of displacements in a quantum, strongly magnetized crystal, at  $\theta \gtrsim 100$ ,  $b \gg 1$ , becomes much larger. The ion displacements are strongly suppressed in the transverse direction and are mildly reduced along the field (see also [24]).

These effects are important for accurate computations of nuclear reaction rates in a strongly magnetized crust of a neutron star (Sec. I). The strongest effect is expected to occur at sufficiently high densities and not too high temperatures in the pycnonuclear burning regime. In that regime (e.g., [12, 13, 14]) the main contribution to the reaction rate comes from the closest neighbors in a crystalline lattice due to their zero-point vibrations. In the field-free case, the rate depends exponentially on the squared ratio of the equilibrium distance between the closest neighbors and the average amplitude of their displacements. The ratio is

typically large, and the reaction rates are exponentially small (but increase with the growth of stellar matter density). Although the reaction rates in magnetized crystals have not been studied yet, one can expect a similar result, involving now the average displacement (39) in the direction of closest neighbors. If so, the rates would become extremely sensitive to the orientation of the magnetic field. If the field is not directed towards one of the nearest neighbors, the reactions will be significantly slowed down by greater tunnelling lengths. Even if the magnetic field is directed towards one of the nearest neighbors then, in addition to the reduction of the longitudinal displacement, there will be a geometrical effect. In a bcc lattice every ion has 8 nearest neighbors, of which only 2 will be located along the magnetic field line. The reactions with the other 6 neighbors will be quenched.

### VIII. PHONON SPECTRUM MOMENTS IN THE MAGNETIC FIELD

According to the well-known Bohr-van Leeuwen theorem, the classical partition function is not affected by the magnetic field. For instance, the classical asymptote of the entropy  $S$  has the form:

$$\frac{S}{3nV} = 1 - \ln \left( \frac{\hbar\omega_p}{T} \right) - \left\langle \ln \left( \frac{\Omega}{\omega_p} \right) \right\rangle_{\text{ph}}. \quad (40)$$

Therefore, the quantity  $\langle \ln(\Omega/\omega_p) \rangle_{\text{ph}}$ , where average over all phonon modes in the first Brillouin zone is implied, *should not depend* on the magnetic field. This statement is easy to prove directly. By inspecting Eq. (10) one concludes that its  $\Omega^0$ -term cannot contain  $B$  at any  $\mathbf{k}$ . On the other hand, this term is equal to  $\Omega_1^2 \Omega_2^2 \Omega_3^2$ , which proves the point.

Phonon frequency moments  $u_m \equiv \langle (\Omega/\omega_p)^m \rangle_{\text{ph}} = u_m(b, \mathbf{n})$  depend on both the field strength and direction  $\mathbf{n}$ . The moment  $u_{-2}$  diverges, while the moment  $u_2 = 1 + b^2$ . Consider the moments  $u_1$  and  $u_{-1}$ . Their dependences on the field strength are shown in Fig. 8(a) for the field direction corresponding to the minimum of the zero-point energy. At strong magnetic fields both moments behave in the same way, proportional to  $b$ , although under the effect of different modes. The main contribution to  $u_1$  comes from the mode  $\Omega_3 \approx \omega_B$ , whereas the major contribution to  $u_{-1}$  is due to the mode  $\Omega_1 \propto 1/B$  (near the center of the Brillouin zone).

The dependence of the phonon frequency moments on the magnetic field direction turns out to be rather weak. In Fig. 8(b) the differences  $\Delta u_1 = u_1(b, \mathbf{n}_2) - u_1(b, \mathbf{n}_1)$  and  $\Delta u_{-1} = u_{-1}(b, \mathbf{n}_2) - u_{-1}(b, \mathbf{n}_1)$  are shown, where  $\mathbf{n}_1$  is the magnetic field direction towards one of the

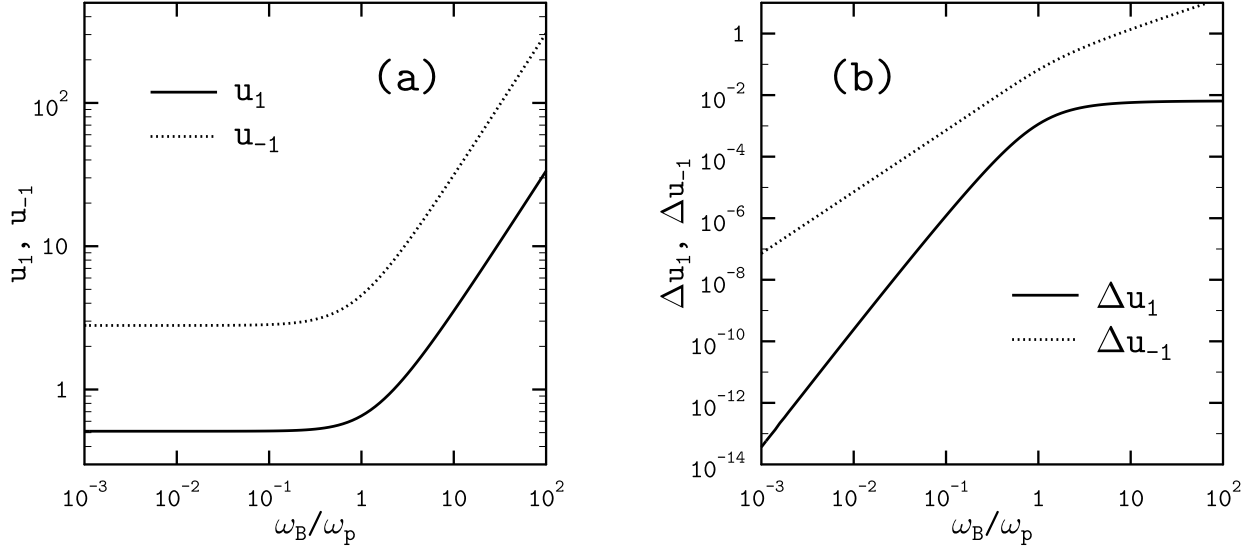


FIG. 8: (a): The dependence of phonon spectrum moments  $u_1$  and  $u_{-1}$  on the strength of the magnetic field directed towards one of the nearest neighbors. (b): The dependence of phonon spectrum moment differences  $\Delta u_1$  and  $\Delta u_{-1}$  on the magnetic field (see explanation in the text).

nearest neighbors, while  $\mathbf{n}_2$  is the direction towards one of the next order nearest neighbors.

The behavior of  $\Delta u_1$  is of special importance because it determines zero-point energy gain  $\Delta E_{\text{zp}} = \frac{3}{2}N\hbar\omega_p\Delta u_1$  resulting from the crystal rotation with respect to the magnetic field. In weak fields  $10^{-3} \lesssim b < 1$ , the difference  $\Delta u_1$  scales approximately as  $b^4$ . In strong fields,  $\Delta u_1$  saturates at a value  $\sim 10^{-2}$ , depending on the field direction. The difference  $\Delta u_{-1}$  scales as  $b^2$  for low magnetic fields, and as  $b$  for strong magnetic fields.

## IX. CONCLUSION

The Coulomb crystal of ions with incompressible charge compensating background of electrons in constant uniform magnetic field has been studied. The phonon mode spectrum of the crystal with bcc lattice has been calculated for a wide range of magnetic field strengths and orientations (Fig. 1). The phonon spectrum has been used in 3D numerical integrations over the first Brillouin zone for a detailed quantitative analysis of the phonon contribution to the crystal thermodynamic functions, Debye-Waller factor of ions, and the rms ion displacements from the lattice nodes for a broad range of densities, temperatures, chemical compositions, and magnetic fields.

The characteristic parameter that determines the strength of the magnetic field effects in the crystal is the ratio of the ion cyclotron frequency to the ion plasma frequency,  $b = \omega_B/\omega_p$ . Even a very strong field ( $b \gg 1$ ) does not alter the partition function (hence, thermodynamic functions, melting etc.) of a classical crystal, i.e. a crystal at a temperature significantly exceeding the energy of any phonon mode ( $T \gg \hbar\omega_B$  for strongly magnetized crystal).

Strong magnetic field dramatically changes various properties of quantum crystals, especially at  $\theta = \hbar\omega_p/T \gg 1$ . Low-temperature phonon specific heat, entropy, thermal energy increase by orders of magnitude (e.g., Figs. 2, 4). The thermodynamic functions exhibit peculiar staircase structures, brought about by the vastly different energy scales of the crystal phonon mode. Ion displacements from the equilibrium positions become strongly anisotropic (Fig. 7), and so does the Debye-Waller factor.

These results can be applied directly to real physical systems found in the crust of magnetars (neutron stars with superstrong magnetic field). In particular, the heat capacity of the magnetized Coulomb crystal composed of fully ionized  $^{56}\text{Fe}$  has been analyzed (Sec. VI). It has been shown that in the magnetic field (as in the field-free case) the phonon heat capacity dominates the electron one in a wide range of densities and temperatures (Fig. 6). In accordance with Sec. V, magnetic field is responsible for a significant boost of phonon heat capacity, which may be important for simulations of magnetar cooling. Since ion displacements are suppressed, one can expect increased crystal stability in the magnetar crust associated with an increase of the melting temperature in the quantum regime. Finally, one expects a reduction of the pycnonuclear reaction rates due to increased tunnelling lengths. The rates are likely to become very sensitive to the orientation of the magnetic field (Sec. VII).

The dependence of thermodynamic functions on the magnetic field orientation within the crystal turns out to be weak, at least for the bcc lattice, but finite. The energy gain, achieved by reorienting the crystal with respect to the magnetic field, can be estimated using Fig. 8.

The techniques used in the present paper can be easily reformulated for fcc lattice, where results are expected to be numerically close to those for bcc lattice.

### Acknowledgments

The author is deeply grateful to D.G. Yakovlev for numerous discussions and valuable comments to the manuscript. This work was partly supported by the Russian Foundation for Basic Research (grant 08-02-00837) and by the State Program “Leading Scientific Schools of Russian Federation” (grant NSh 2600.2008.2).

- 
- [1] E.P. Wigner, Phys. Rev. **46**, 1002 (1934).
  - [2] D. Pines, *Elementary Excitations in Solids* (Mir, Moscow, 1965).
  - [3] W.M. Itano, J.J. Bollinger, J.N. Tan, B. Jelenković, X.-P. Huang, and D.J. Wineland, Science **279**, 686 (1998); D.H.E. Dubin and T.M. O’Neil, Rev. Mod. Phys. **71**, 87 (1999).
  - [4] G. Chabrier, N.W. Ashcroft, and H.E. DeWitt, Nature **360**, 48 (1992).
  - [5] P. Haensel, A.Y. Potekhin, and D.G. Yakovlev, *Neutron Stars. 1. Equation of State and Structure* (Springer, New York, 2007).
  - [6] D.A. Baiko, A.Y. Potekhin, and D.G. Yakovlev, Phys. Rev. E **64**, 057402 (2001).
  - [7] D.E. Winget, S.O. Kepler, F. Campos, M.H. Montgomery, L. Girardi, P. Bergeron, and K. Williams, Astrophys. J. Lett. **693**, L6 (2009).
  - [8] T.S. Metcalfe, M.H. Montgomery, and A. Kanaan, Astrophys. J. **605**, L133 (2004).
  - [9] D.A. Baiko, A.D. Kaminker, A.Y. Potekhin, and D.G. Yakovlev, Phys. Rev. Lett. **81**, 5556 (1998).
  - [10] A.I. Chugunov and D.G. Yakovlev, Astron. Rep. **49**, 724 (2005).
  - [11] A.D. Kaminker, C.J. Pethick, A.Y. Potekhin, V. Thorsson, and D.G. Yakovlev, Astron. Astrophys. **343**, 1009 (1999).
  - [12] E.E. Salpeter and H.M. Van Horn, Astrophys. J. **155**, 183 (1969).
  - [13] D.G. Yakovlev, L.R. Gasques, M. Beard, M. Wiescher, and A.V. Afanasjev, Phys. Rev. C **74**, 035803 (2006).
  - [14] A.I. Chugunov and H.E. DeWitt, Phys. Rev. C **80**, 014611 (2009).
  - [15] C. Thompson, Mem. Soc. Astron. Ital. **73**, 477 (2002).
  - [16] P.M. Woods and C. Thompson, in *Compact Stellar X-ray Sources*, edited by W.H.G. Lewin and M. van der Klis (Cambridge Univ. Press, Cambridge, 2006), p. 547.

- [17] V.M. Kaspi, in *Young Neutron Stars and Their Environments*, edited by F. Camilo and B.M. Gaensler (Astron. Soc. Pacific, San Francisco, 2004), p. 231.
- [18] SGR/AXP Online Catalog: <http://www.physics.mcgill.ca/~pulsar/magnetar/main.html>
- [19] A.L. Watts and T.E. Strohmayer, *Adv. Space Res.* **40**, 1446 (2007).
- [20] D.A. Baiko, Ph.D. thesis, A.F. Ioffe Physical–Technical Institute, 2000.
- [21] A.Y. Potekhin, G. Chabrier, and D.G. Yakovlev, *Astron. Astrophys.* **323**, 415 (1997).
- [22] N.A. Usov, Yu.B. Grebenshikov, and F.R. Ulinich, *ZhETF* **78**, 296 (1980).
- [23] T. Nagai and H. Fukuyama, *J. Phys. Soc. Jap.* **51**, 3431 (1982).
- [24] T. Nagai and H. Fukuyama, *J. Phys. Soc. Jap.* **52**, 44 (1983).
- [25] D.A. Baiko, *Phys. Rev. E* **66**, 056405 (2002).
- [26] M.H. Cohen and F. Keffer, *Phys. Rev.* **99**, 1128 (1955).
- [27] E.L. Pollock and J.P. Hansen, *Phys. Rev. A* **8**, 3110 (1973).
- [28] L.D. Landau and E.M. Lifshitz, *Statistical Physics* (Butterworth-Heinemann, 1984).
- [29] R.C. Albers and J.E. Gubernatis, Los Alamos Scientific Laboratory Report, 1981.
- [30] M. Born and K. Huang, *Dynamical Theory of Crystal Lattices* (Clarendon Press, Oxford, 1954).
- [31] G. Wunner, H. Ruder, and H. Herold, *Astrophys. J.* **247**, 374 (1981).
- [32] A.Y. Potekhin, *J. Phys. B: At. Mol. Opt. Phys.* **31**, 49 (1998).